Spatial distribution of B cells predicts prognosis in human pancreatic adenocarcinoma

Oncoimmunology , 2016, ahead of Print ; **DOI:**10.1080/2162402X.2015.1085147

UNIVERSITÀ DEGLI STUDI DI TORINO

Oncoimmunology , 2016, ahead of Print ; **DOI:**10.1080/2162402X.2015.1085147

Distribution of B cells within tertiary lymphoid tissue predicts prognosis in human pancreatic cancer

Giovanni Francesco Castino[1], Nina Cortese[1], Giovanni Capretti[2], Simone Serio[3], Giuseppe Di Caro[1], Rossana Mineri[4], Elena Magrini[1], Fabio Grizzi[1], Paola Cappello[5], Francesco Novelli[5], Cristina Ridolfi[4], Francesca Gavazzi[4], Alessandro Zerbi[4], Paola Allavena[1], Alberto Mantovani[1], Federica Marchesi[1,6]

[1] Department of Immunology and Inflammation, Humanitas Clinical and Research Center, Rozzano, Italy

[2] Section of Pancreatic Surgery, Department of Surgery, Humanitas Clinical and Research Center, Rozzano, Italy

[3] Operational Unit of Milan, Institute of Genetics and Biomedical Research, National Research Council and Humanitas Clinical and Research Center, Rozzano, Italy

[4] Molecular Biology Section, Clinical Investigation Laboratory, Humanitas Clinical and Research Center, Rozzano, Italy

[5] Center for Experimental Research and Medical Studies, Città della Salute e della Scienza di Torino and Department of Molecular Biotechnology and Health Science, University of Torino

[6] Correspondence to federica.marchesi@humanitasresearch.it

Abstract

In this study, we investigated the role of B cells in the microenvironment of human PDAC, in a retrospective and consecutive cohort study involving a series of 104 PDAC patients and in PDAC preclinical models. Analysis of PDAC tissues by immunohistochemistry revealed two distinct patterns of B cell distribution, either as randomly infiltrating cells (CD20-TILs), or strategically located within organized tertiary lymphoid tissue (CD20-TLT). The two B cell components displayed divergent immune profiles and opposite prognostic relevance. Notably, high density of CD20-TLT associated to a germinal center immune signature, correlated with CD8-TIL infiltration, and empowered their favorable prognostic value. The presence of PD1+ follicular helper T cells (Tfh) within CD20-TLT correlated with increased density of TLT and the two immune variables together identified a subgroup of patients with better prognosis. Vaccination of $KRas^{G12D}$/Cre mice with ENO1, a pancreatic tumor antigen, induced formation of intra-tumoral TLT with active germinal centers and correlated with increased recruitment of T cells, suggesting induction of TLT as a strategy to favor localization of immune cells in PDAC. In contrast, in an implanted tumor model devoid of TLT, depletion of diffuse B cells with an anti-CD20 antibody reinstated an antitumor immune response. Our results highlight B cells as an essential element of the microenvironment of PDAC, but with divergent roles according to their localization. A mindful evaluation of B cells in human PDAC could represent a powerful prognostic tool to identify patients with distinct clinical behaviors and responses to immunotherapeutic strategies.

INTRODUCTION

Pancreatic ductal adenocarcinoma (PDAC) is the fifth cause of cancer worldwide (1). Approximately, only 20% of patients are eligible to surgery and standard-care therapies have limited impact on survival (2), fostering the efforts towards complementary anticancer strategies, including immunotherapy. PDAC-associated immune contexture has been described, both in genetic mouse models and human PDAC, as a desmoplastic stroma mainly composed of immunosuppressive cells (3), since the very early phases of the disease (4) and representing a barrier to both chemotherapeutic drugs (5) and effector T cells (6), as well as a target of immunotherapeutic approaches (7). This view has recently been challenged by studies revealing a positive effect of PDAC stroma to immunotherapeutic strategies (8, 9), thus reinforcing the hypothesis that a better definition of the immune environment of PDAC would help identifying patients who are more likely to benefit from immunotherapeutic approaches (4, 10, 11).

In the era of personalized cancer medicine and innovative immunotherapeutic strategies, translational research has been challenged with the need of informative biomarkers to better stratify tumor patients and choose the optimal therapeutic treatment accordingly (12). Tumor profiles generated by standardized wide-scale analyses have highlighted a central position of immune variables in dictating tumor progression (12-14), suggesting that specific immune subsets should be included within currently available TNM staging in the determination of patient's prognosis (15, 16). Despite the advent of innovative prognostic tools, such as global molecular analyses, histo-pathological examination of immune infiltrates in tumor tissues still stands as one of the most powerful approaches to assess the relevance of the immune microenvironment.

Within the tumor microenvironment, the spatial orientation of immune cells has emerged as important determinant of immune cell function (17). According to the localization and distribution of lymphocytes within tumors, various components of the intra-tumor lymphocytic reaction can be identified, including peri and intra-tumor infiltration, diffuse infiltration and, more recently defined, organization into ectopic lymph node structures (or tertiary lymphoid tissue, TLT) (16, 18-22).

Spatial compartmentalization of lymphocytes within TLT is crucial for recruitment of tumor infiltrating T lymphocytes (TILs) (16, 22, 23), T cell activation and germinal center reactions (24, 25), and has been shown to coordinate with TIL infiltration in predicting better clinical outcome (16, 26). Even though B cells represent an important component of the immune infiltrate in solid tumors (27-32) and a major cellular constituent of TLT, the role of tumor infiltrating B cells has been only marginally addressed, mainly because B cells infiltrate the tumor microenvironment in smaller numbers compared to T cells and other leukocyte populations. Thus, a definition of B-cell functions in the progression of human cancer is still object of intense study. B cell activation requires proper help from follicular helper T (Tfh) cells, the T cell subset residing in the B cell area of lymphoid tissue and deputed to induce B cell differentiation into immunoglobulin-producing cells (33, 34). Tfh home to B cell follicles within lymphoid organs to support antibody responses and are key regulators in germinal center (GC) reactions, regulating B cell survival and affinity maturation within GC (35-37). Compared to other CD4+ T cell subsets, Tfh cells distinctly express the transcription factor B cell lymphoma 6 (Bcl-6), co-stimulatory molecules including programmed cell death 1 (PD1) and inducible costimulator (ICOS) and high levels of IL-21 and CXCL13, important molecules to shape B cell responses. Their role in anti-tumor immune responses has been recently proposed (38).

In this work, with an accurate and systematic assessment of specific immune variables, we analyzed B cells infiltrating human PDAC. We found B cells in two histologically distinct components, either within tertiary lymphoid tissue (B-TLT) or interspersed at the tumor-stroma interface (B-TILs). In a large mono-institutional cohort of 104 surgically resected PDAC patients, the two B cell components identified subpopulations of PDAC patients with specific immune signatures and clinical behaviors. Our results highlight the central role of B cells in the progression of human PDAC and the importance of an accurate evaluation of the *in situ* immune reaction.

RESULTS

Distinct histological patterns of B cells in human PDAC. Human pancreatic adenocarcinoma is conventionally considered non-immunogenic, due to immune exclusion and a prominent infiltration of T–regulatory and immunosuppressive myeloid cells (3, 7). Interestingly, immunohistochemistry analysis of human PDAC specimens with an anti-CD20 antibody revealed a considerable infiltration of B cells (**Figure 1A**). CD20+ cells localized not only as interspersed cells at the tumor-stroma interface (CD20-TILs) (arrowheads in **Figure 1A** and **Figure 1B**), but also as a component of dense aggregates displaying a distinct structural organization and located in the tumor stroma (asterisks in **Figure 1A** and **Figure 1C**). These structures resembling tertiary lymphoid tissue (CD20-TLT) were not present in the normal pancreatic tissue (not shown), thus suggesting that their neo-genesis is related to tumor occurrence. Importantly, B cells infiltrating human PDAC were preferentially located within TLT (CD20-TLT); in fact, density of B cells in TLT was significantly higher compared to density of scattered CD20-TILs ($P<0.0001$; **Figure 1D**). A more detailed characterization of CD20-TLT aggregates revealed an organization similar to lymph-nodes, with B cells (**Figure 1E**) and T cells (**Figure 1F**) partitioned in topologically distinct areas, containing CD8+ lymphocytes (**Figure 1G**) and mature dendritic cells expressing DC-LAMP (**Figure 1H**). An organized network of specialized PNAd+ high endothelial venules (HEV) (arrowheads in **Figure 1I**) and lymphatics (arrowheads in **Figure 1J**) confirmed that they have features of tertiary lymphoid tissue (TLT). The presence within lymphoid tissue of the lymph-organogenic chemokines CXCL13 (**Figure 1K**) and CCL21 (**Figure 1L**), involved in recruitment of B and T cells and in their topological segregation, suggests an immunological task for TLT in the microenvironment of human PDAC.

Dichotomy of B cell prognostic impact in human PDAC. The dual histological distribution of B cells within pancreatic tissue suggests that they could have distinct functions. We then addressed the clinical significance of B cells in human PDAC considering CD20-TLT and CD20-TILs as peculiar populations. In a retrospective cohort study, we quantitatively evaluated the density of the

CD20-TLT and CD20-TILs at the tumor-stroma interface of 104 tissue specimens from consecutive, non-metastatic PDAC patients. Distributions of immune populations according to the patient histo-pathological characteristics are described in **Supplementary Table 1**. Considering the overall cohort, TLT immune-reactive area (IRA%) ranged from 0.00% to 23.49%, with a median value of 3.72% (second–third quartiles, 1.71%-5.71%) (**Supplementary Table 1**). We recorded 38 events of disease specific death (DSS) in 104 PDAC patients. Cox multivariate analysis showed that nodal status and grade associated to prognosis; notably, among the immune variables analyzed, B cells were independently associated to prognosis, but their prognostic value diverged according to their distribution, since CD20-TLT associated with better prognosis (p=0.010, 3^{rd} -4^{th} versus 1^{st} quartile; **Table 1**), while CD20-TILs associated to worse prognosis (P=0.040, 3^{rd} versus 1^{st} quartile; **Table 1**). This result highlights B cells as prognostic variables in human PDAC and suggests that the influence of B cells on tumor progression changes whether they are confined within lymphoid tissue or are scattered at the tumor-stroma interface. In accordance, Kaplan-Meier survival analysis showed that while high density of CD20-TLT (1^{st} versus 2^{nd}-4^{th}) correlated to better prognosis (P=0.0085; n=104; **Figure 2A**), CD20-TIL density (1^{st}-2^{nd} versus 3^{rd}-4^{th}) had a propensity to associate to worse prognosis albeit not significant (P=0.115; n=104; **Figure 2B**). Most importantly, the immune signature comprising CD20-TLT^{hi} /CD20-TIL^{lo} robustly predicted longer survival (P=0.0051; n=104; **Figure 2C**), confirming that the histological architecture of B cells dictates their prognostic behavior, with only B cells sequestered within a lymphoid tissue contrasting tumor progression.

Confinement of B cells within TLT associates to a germinal center immune signature, correlates with CD8-TIL infiltration, and empowers their favorable prognostic value. To understand how B cells dually regulate tumor progression according to their distribution, we analyzed the immune signature of PDAC tumors from TLT^{hi} (4^{th} quartile) patients compared to TLT^{lo} (1^{st} quartile) patients, by mRNA expression analysis of paraffin-embedded tissue specimens. Normal pancreatic tissue, adjacent to tumor region, was taken as control tissue. Hierarchical clustering analysis revealed stable groupings by type of immune infiltrate (**Supplementary Figure**

1), with TLT^{hi} versus TLT^{lo} samples segregating together, suggesting that classification of tumor specimens according to the density of CD20-TLT identifies specific gene expression programs. Compared to normal pancreatic tissue, PDAC specimens with high density of TLT showed major changes in genes related to B-cell differentiation and proliferation (interleukin-7 (*IL7*)) and B-cell responses (*IL4, IL5, IL13*), germinal center reaction (activation-induced cytidine deaminase (*AICDA*), inducible T-cell costimulator ligand (*ICOSL*)), B-cell signaling (B-cell linker (*BLNK*), lymphocyte-specific protein tyrosine kinase (*LCK*)) and B cell recent activation (*CD27*) (**Figure 3A**). Surprisingly, TLT^{hi} PDAC samples exhibited a significant increase in genes related to T-cell infiltration (*CD8A*, *CD8B* and *CD4*) and activation (*IL-12*, *IL12RB1*, *CD86*, *CD40L*) (**Supplementary Figure 1**), suggesting that the presence of B cells within TLT was also regulating T cell recruitment and activation. Immunohistochemical analysis confirmed that B cells within TLT were often engaged in a germinal center reaction, as evidenced by Bcl-6 (arrowheads in **Figure 3B, upper panel**) and Ki67 immunostaining (arrowhead in **Figure 3B, lower panel**).

CD8+ T cells are a essential constituent of the antitumor immune response in the microenvironment. In light of the association between TLT^{hi} and CD8 in gene expression analysis, we assessed the density of tumor-infiltrating CD8+ T-cells (CD8-TILs) in the 104 PDAC patients (**Supplementary Figure 2**). Notably, whole tissue visualization of CD8+ infiltrating cells evidenced a higher density of CD8-TILs in tissues with a high density of TLT (arrowheads in **Figure 3C)**. In fact, density of CD20-TLT linearly correlated with the density of CD8-TILs (r=0.29, p=0.009, n=104) (**Figure 3D**), consistent with the ability of TLT to mediate recruitment of lymphocytes (16). Most important, while CD8-TILs were not associated to prognosis on their own (P=0.254, n=104) (**Table 1** and **Figure 3E**), concomitant high density of CD8-TILs (2^{nd}-4^{th} quartiles) and high density of TLT (2^{nd}-4^{th} quartiles) identified a subgroup of patients with better outcome compared to other patients (p=0.031, n=104) (**Figure 3F**), suggesting that the presence of tertiary lymphoid tissue empowers the prognostic function of CD8+ T cells.

PD-1^{+} follicular helper T cells within TLT germinal centers regulate the balance between B-cell protumor and antitumor prognostic value. We then moved on to investigate specific

elements inside TLT could have a role in B cell dual function. Within the B-cell zone of TLT (**Figure 4A**), it was often possible to distinguish a distinct structure resembling a germinal center (GC), characterized by the presence of PD-1+ cells (**Figure 4B**). This suggests that they could be T-helper follicular cells (**Figure 4C**), an important subset of T cells with a key role in the germinal center reaction and B cell activation (33, 34). To investigate whether the presence of this particular subset within the germinal center of TLT could have an impact on B cell prognostic function, we systematically quantified the germinal centers expressing PD-1 (PD1-GC) in the cohort of 104 PDAC patients. PD-1-GC cells were present in 32 out of 104 patients (30.8%). Notably, comparing PDAC specimens with and without PD1-GC cells, the number of patients with high density of TLT was significantly higher in the PD1-GC group compared to specimens with low density of TLT ($p<0.0001$), suggesting that the presence of this subset is key to the formation of TLT within the tumor microenvironment (**Figure 4D**). Surprisingly, in patients with PD-1-GC there was no correlation of CD20-TLT with CD20-TILs ($r=-0.001$, $P=0.559$, $n=32$) (**Figure 4E**), while the two B cell components correlated in specimens without PD1-GC ($r=0.39$, $P=0.001$, $n=70$) (**Figure 4F**), suggesting that the presence of PD1-GC cells could be an important factor favoring B cell aggregation in TLT and preventing B cell scattering within the tissue. Interestingly, multiple linear regression analysis revealed that the density of CD20-TLT did not linearly correlate with the density of CD20-TILs among PDAC patients with good prognosis ($r=0.31$, $p=0.109$, $n=66$), while the two B-cell variables correlated among patients with poor prognosis ($r=0.47$, $p=0.035$, $N=38$) (**Supplementary Figure 3**), suggesting that only B cells sequestered within TLT critically inhibit tumor progression, while the presence of B cells within the tumor tissue seems detrimental to the disease.

Importantly, a concomitant presence of PD1-GC cells and high TLT (2^{nd}-4^{th} quartiles) (**Figure 4G**) identified a subgroup of patients with a significantly better prognosis ($p=0.027$, $n=102$). This data suggests that Tfh cells are decisive determinants of TLT formation and B cell retention within TLT, and that PD-1-GC cells could strongly contribute to the organization of an antitumor immune response in human PDAC.

Antigen-specific immunotherapeutic vaccination induces neogenesis of intratumor TLT with PD-1+ germinal centers in a preclinical model of PDAC. The presence of immunological active TLT could be of remarkable importance in the perspective of inducing a local antitumor humoral immune response. Several immunotherapeutic approaches are under study in human PDAC, including vaccination protocols directed against PDAC antigens, which would benefit from a microenvironment favorable for TLT induction. We therefore investigated whether a DNA vaccination could induce formation of TLT in a genetic preclinical model of PDAC. Vaccination of tumor-bearing mice with a vector encoding α-enolase (ENO1) has been shown to have a protective effect in KrasG12D/Cre mice (39). Immunohistochemical analysis of PDAC tumors confirmed the sporadic occurrence of TLT in PDAC tumors. However, mice injected with ENO1-vaccine had a significant increase of number and area of TLT, compared to both untreated and mice injected with empty vector (**Figure 5A-B**), suggesting that boosting the immune response with vaccination induces recruitment and organization of lymphocytes in the microenvironment. Remarkably, analysis of PD1-GC highlighted a robust increase in ENO1 mice compared to control (**Figure 5C-D**), demonstrating that vaccination is able to break the immunosuppressive barrier, inducing a specific in situ immune reaction .The increase was paralleled by an increase in CD3-TILs, suggesting that induction of TLT by immunotherapeutic approaches could be a strategy to increase recruitment of T cells (**Figure 5E-F**). Importantly, vaccination resulted in long-lived systemic protective immunity, as evidenced by a rise of circulating rENO1-specific antibodies in ENO1-vaccinated mice compared to mice vaccinated with the empty vector (**Figure 5G**).

Targeting tumor infiltrating B cells unleashes the antitumor immune response in murine PDAC. For their key role in the pathogenesis of immune diseases, including cancer, B cells represent feasible therapeutic targets to inhibit harmful humoral immune responses (30). However, our data showing the dual role of B cells in human PDAC raises some concern for the targeting of B cells in solid tumors. To clarify this point, we tested the effect of a mouse anti-mouse CD20 antibody targeting B cells (clone 5D2, Genentech) in an implantable model of PDAC, by injecting the antibody 3 days post tumor injection. We did not observe formation of B-TLT in any of the

orthotopically implanted mice (**Supplementary Figure 4**), likely due to the rapid tumor growth (21 days) and absence of chronic inflammatory reaction. In contrast, scattered B cells (B-TILs) infiltrated the tumor tissue (**Supplementary Figure 4**), confirming in this preclinical model that B-TILs act independently from B-TLT. Circulating B cells were dramatically depleted by a single injection of the antibody (**Figure 6A**), and the effect persisted until the end of the experiment (**Figure 6B**), while the number of other circulating leukocytes (including CD3+ T cells and CD11b+ myeloid cells) was not significantly affected (**Supplementary Figure 5**). Consistent with the reduction of circulating B cells, the number of B220-TILs scattered in the tumor microenvironment was significantly reduced by the treatment (**Figure 6C-E**), suggesting that B220-TILs are recruited from a circulating pool of B cells. Notably, single injection of anti-CD20 slightly reduced the tumor size, albeit not significantly, suggesting a protumor function of B-TILs in PDAC (**Figure 6F**).

To analyze the impact of B-TIL depletion, we compared the immune signature of the leukocyte population isolated from PDAC tumors from control and α-CD20 treated mice. Interestingly, depletion of tumor infiltrating B cells resulted in a significant increase in genes related to T cell and NK cell infiltration (*CD4*, *CD8*, *NCR1*), activation (*GMZ-A*, *GMZ-B*, *IL-12, IFN-g,* and *TNF-alpha*) and recruitment (*CXCR3*) (**Figure 6G**). These results show that, in an implanted tumor model devoid of B220-TLT, depletion of tumor infiltrating B cells (B-TILs) increases the recruitment of important components of the antitumor immune response. This was not ascribable to a compensatory increase of circulating T cells, which were not significantly affected by the α-CD20 treatment (**Supplementary Figure 5**).

To gain more insights on the biological relevance of the signature obtained, we interrogated the set of genes by a systems biology approach based on Ingenuity Pathway Analysis (IPA). Surprisingly, within the panel of genes analyzed (**Supplementary Figure 6**), depletion of B cells with α-CD20 induced significant functional enrichment of genes involved in lymphoid tissue structure and development, CD8+ T cell infiltration and maintenance and differentiation of T cells (**Figure 6H**), confirming that B-TILs are detrimental to an effective antitumor immune response.

DISCUSSION

In the last decade, the immune microenvironment has gained attention as a source of novel biomarkers of clinical outcome and targets of therapeutic intervention (12-14, 40). However, the lack of adequate systematic approaches to evaluate immune cells has hindered the introduction of immune variables into clinical practice. In this context, the spatial orientation regulating immune cell function within the tumor tissue has only recently begun to be taken into consideration. We and others have demonstrated that the organized distribution of B and T lymphocytes into tertiary lymphoid tissue favors the recruitment of T cells and associates to an anti tumor immune response, predicting better patient outcome in human cancer patients (16, 22, 41, 42).

In the present work, we moved on to analyzing the B cell component in human PDAC, in the prospect of identifying specific immune variables indicating clinically relevant immune responses. Unexpectedly, our analysis evidenced a dual prognostic behavior of B cells, which is tightly linked to their topological distribution within the microenvironment. Rather than scattered in the tumor tissue, the majority of B cells was found strategically located in association with T cells, within highly organized lymphoid tissue, possibly reflecting how B and T cells interact during the organization of a local immune response. Only when confined within a lymphoid site equipped with a germinal center B cells predicted better prognosis, suggesting that they might be involved in an ongoing follicular immune response with a protective antitumor role, while presence of B cells outside the germinal center is not essential to their antitumor function. This is in sharp opposition to what observed for T cells, whose localization at the tumor invasive margin is critical to predict better prognosis (16). In contrast, the correlation of TLT with B cells among patients with worse prognosis further suggests that the egress of B cells into the tissue is detrimental to an effective antitumor response and might reflect a non-specific protumor inflammatory reaction. The role of B cells in the progression of solid tumors has fostered studies concerning their targeting by anti-CD20 antibodies. Based on our data, the design of anticancer strategies envisaging the depletion of B cells should take into account the possibility to selectively target CD20-TILs but not CD20-TLT. Interestingly, in non–tumor conditions, anti-CD20 therapy has resulted ineffective in depleting

CD20+ cells in tertiary lymphoid organs (43), suggesting that B cells might receive survival signals within TLT. The differential sensitivity of the distinct B cell components to anti-CD20 treatment could be exploited to design tailored approaches, assuming that a rigorous evaluation of B cells is performed.

Specific activated immune cell subsets within TLT have been shown to be associated to patient prognosis (26). In our analysis, we identified PD1 expressing Tfh cells as a critical subset of T cells within TLT, likely involved in the immune function and identifying a subgroup of patients with favorable outcome. Tfh cells take part in various steps leading to germinal center reaction and differentiation of memory B cells and plasmacells (36, 44). Our data suggest that TLT able to successfully enclose B cells into Tfh-containing germinal centers correlate to better prognosis as they more effectively contribute to a protective immune response. The PD-1/PD-1L network is emerging as a major inhibitory pathway associated with T cell exhaustion in the tumor microenvironment (45, 46); our data that PD-1 expression correlates with better prognosis is counterintuitive considering the ongoing efforts aimed at targeting this inhibitory pathway in human cancers. However, while PD-1 expression in peripheral tissues associates to immunosuppressive function, PD-1 upregulation in lymphoid tissues is an early event of T cell activation and identifies clonally expanded tumor reactive T cells (47). Therefore, PD1 expression in germinal centers within TLT could indicate the functional competence of the lymphoid aggregates and T cell recent activation, irrespective of its immunosuppressive role when engaged by the ligand, eventually suggesting that immunotherapeutic strategies targeting PD-1 could concomitantly act on exhausted T cells as well as enhance recently activated T cells. As for B cells, our data suggest that a careful evaluation of immune cells within the microenvironment is required in order to allocate the best therapeutic treatment.

Immunotherapeutic approaches for PDAC are a promising alternative option to the scarcely effectual available treatments, but still far from being successfully adopted in the clinic (48). The immunosuppressive nature of the tumor microenvironment (49) and the defective localization of adoptively transferred immune cells at the tumor site (40) have blunted the efficacy of

immunotherapy, favoring T-cell exclusion and immune ignorance. The presence of an ectopic lymphoid site as TLT could overcome these obstacles by providing a local immune site favoring antigen presentation and sustaining lymphocyte traffic. Moreover, the association of TLT with better prognosis suggests that the immune response induced could be protective overtime.

The identification of histologically distinct immune components, i.e. PD1-GC and CD20-TLT, which concur in classifying PDAC patients according to clinical behavior is expected to have important implications in the design of clinical trials aimed at testing innovative immunotherapeutic approaches. Moreover, the objective and compartment-specific evaluation of immune populations we provided allows envisaging TLT as a promising prognostic tool in clinical practice for PDAC patients. Our analysis brings to light the critical duality displayed by immune cells according to their spatial orientation in the tumor microenvironment, raising criticism about studies addressing the prognostic role of immune cells obtained by gene expression-based or FACS-based analyses and underlines the need of an integrated analysis of the immune microenvironment.

From a clinical perspective, the assessment of TLT might represent a potential approach to better allocate patients to immunotherapy (50). In this regard, our data diverges from the general view that the PDAC microenvironment is mostly devoid of infiltrating lymphocytes and from recent evidence showing that an immunotherapeutic protocol induced TLT in human PDAC patients, otherwise devoid of TLT (51). In our considerable cohort, TLT occurrence was observed in a high percentage of patients, to variable extents, suggesting that the microenvironment of human PDAC is in fact permissive to the infiltration of lymphocytes and that strategies either enhancing their formation or activation status should be encouraged.

MATERIALS and METHODS

Patients and study design

The cohort study included 104 patients aged older than 18 years, diagnosed with pancreatic ductal adenocarcinoma (PDAC) and who consecutively underwent surgery with curative intent at Humanitas Clinical and Research Center, from February 2010 to December 2012. Investigators were blinded to the results of the analysis and assembled a clinical retrospective database by collecting patient demographics, clinical, and histopathological data from the institutional intranet, as detailed in **Supplementary Table S1.** Patients with metastases at surgery (n=7) were excluded from the analysis. Detection of postsurgical local and distant tumor recurrences included a baseline thoracic and abdominal computed tomography (CT) and CA19-9 evaluation. CT was repeated every 3 months during the first 2 years after surgery, and every 6 months afterward. CA19.9 assessment was repeated on a monthly basis during chemotherapy and concomitantly to CT scan afterward. As outcome variable we considered disease-specific survival (DSS), defined as any PDAC-related death detected in the observational period started immediately after surgery. Patients who died from causes other than PDAC were considered as negative outcome. The time of DSS was calculated from the date of surgery until date of death. The mean follow-up period of the cohort studied was 563.4 days (Standard Deviation = 320.8 days).

Immunohistochemistry

Human FFPE-PDAC tissues were provided as tissue blocks, by the anatomical pathology division of the Humanitas Clinical and Research Center. 2μm thick consecutive tissue slides were obtained from each block and stained as previously described (16). Slides were autostained (IntelliPATH FLX; Biocare Medical) with primary antibodies raised against CD20 (DAKO, L26), CD8 (DAKO, C8/144B), PD-1 (Abcam NAT105), or manually stained using CD3 (DAKO, F7.2.38), DC-Lamp (Dendritics, 1010E1.01), PNAd (BD Pharmingen, MECA-79), Lyve-1 (Abcam, polyclonal), CXCL13 (R&D, polyclonal), CCL21 (R&D, polyclonal), IL-10 (R&D Systems, polyclonal), Ki67 (DAKO, MIB-1), Bcl-6 (DAKO, PG-B6p) as primary antibodies. Immunohistochemistry was performed with the same protocol on FFPE tissues from mouse pancreata. Primary antibodies used were: B220 (ebioscience, RA3-6B2), PD-1 (Novus Biologicals, polyclonal), CD3 (ebioscience, 145-2C11).

Image analysis

After staining procedure, tissue slides were digitalized using dotSlide (Olympus dotSlide). At least two independent operators blinded to any patient clinical data randomly selected three non-contiguous microscopic areas comprising of approximately 50% of tumor and 50% of stromal tissue and including CD20-TILs and CD8-TILs. For CD20-TLT analysis, 3 non-contiguous fields were chosen representing the entire CD20 positive area within the TLT, regardless of the location in the tumor or in the stroma. The dimension of the microscopic area was maintained fixed throughout the analysis of all mentioned variables. Selected areas were quantified by computer-assisted image analysis, with ad hoc created software, to obtain the percentage of immune reactive areas (IRA%) of the digitalized tissue surface. Mean values, obtained for each variable analyzed in the three different regions were calculated. The variable PD1-GC was expressed as a dichotomous value, assigning a positive value when PD1 positive cells were present in the germinal center of previously assessed CD20-TLT. The extent of the overall distribution of CD20-TLT, CD20-TIL, CD8-TIL IRA%, expressed as continuous variables, and PD1-GC score were used to perform statistical analyses. For each immune variable with continuous values (CD20-TLT, CD20-TILs, CD8-TILs), we first stratified patients by grouping into quartiles, which were further combined to achieve statistically significant groups. By this way, the 1st quartile group and the 2nd-4th quartile group identified two distinct outcome-based groups for CD20-TLT and CD8-TILs, while for CD20-TILs 1st-2nd versus 3rd-4th quartiles were grouped.

Statistical analysis

The associations between values of CD20-TLT, CD20-TILs, CD8-TILs, PD-1-GC and other features concerning patient clinical conditions were estimated by Pearson simple linear regression analysis. A multivariate Cox proportional hazards model was developed to assess the role of

immune variable density and demographic, clinical, and histopathologic features, in predicting the outcome of disease specific survival. To assess for confounders, COX multivariate analysis was performed by the enter approach, entering only variables and their significant interactions with a P value less than 0.05 at Cox univariate analysis. Kaplan–Meier curves of DSS were plotted and the log-rank test was used to compare the curves of each subgroup of patients with pancreatic cancer. For each test, only two-sided P values lower than 0.05 were considered statistically significant. All the analyses were done using SPSS (Version 22.0) and GraphPad Prism software (Version 4.1). To study the prognostic value of immune variables, we adhered to "Reporting Recommendations for Tumor Marker Prognostic Studies (REMARK)" (52) for high quality of tumor marker studies.

Gene expression analysis

Patients were divided into TLT^{hi} (4th quartile) and TLTlo (1st quartile), according to CD20-TLT IRA% values and RNA extracted from formalin-fixed paraffin embedded **(**FFPE) tissues using the RNeasy FFPE kit (QIAGEN). RNA from Panc02 tumors was extracted after collagenase (Sigma Aldrich) digestion of tumor fragments and isolation of the leukocyte fraction by gradient centrifugation (Percoll (GE Healthcare life sciences)). Cells were resuspended with PureZOL (Bio-Rad), and RNA was purified using RNeasy Plus Mini kit (QIAGEN) following manufacturer instructions. In both cases, cDNA was obtained after a 8 cycles pre-amplification step, followed by reverse transcription with the RT^2 PreAMP cDNA synthesis kit (Qiagen). Real-Time PCR was performed using commercially available PCR Arrays (RT^2 ProfilerTM PCR Array System, Qiagen), on a ViiA™ 7 Real-Time PCR (Life Technologies). Differences in gene expression were analyzed by the comparative threshold cycle (Ct) method with DataAssist^{TM}, after global normalization. 5 samples of PDAC tumors from TLT^{hi} (4th quartile) patients and 4 samples of PDAC tumors from TLT^{lo} (1st quartile) patients were analyzed. Within a specific group, samples with the lowest Ct variability (n=3) were selected for analysis (**Supplementary Figure 7**). Adjacent normal pancreatic tissue (n=3) was used as a control. Hierarchical clustering was performed with the Cluster 3.0 software, including the whole gene-list available in the Array. The normalized signal value was adjusted to log transform data and "median" was selected to center genes. Clustering was performed using the euclidian distance function with Java Tree View and exported to heatmap images. For the network analysis, uploading control and aCD20-treated data set, containing gene identifiers and corresponding expression values, into the Ingenuity Pathways Analysis application generated significant pathways and molecular networks. The resulting Network Eligible molecules were overlaid onto a global molecular network based on the in Ingenuity's Knowledge Base (Ingenuity® Systems, www.ingenuity.com). The Functional Analysis of the network identified the biological functions most significant to the molecules in the network.

PDAC murine models

All mice used for the orthotopic implantation of Panc02 cells were 8-week-old C57BL/6J females purchased from Charles River (Calco, Italy) and housed in a specific pathogen–free animal facility of the Humanitas Clinical and Research Center, in individually ventilated cages. Procedures involving animals and their care were conformed to EU and Institutional Guidelines. Murine Panc02 cell line was kindly provided by Dr. Piemonti (San Raffaele Hospital, Milan) and cultured in RPMI 1640 medium (Lonza) supplemented with 10% FBS, 2 mM l-Glutamine. Cells were cultured in a humidified incubator with 5% CO_2, for one passage before *in vivo* injection. Mice were kept anesthetized during all surgical operation by intraperitoneal administration of a ketamine and xylazine solution. The stomach and the adherent pancreas were exteriorized to expose the head of the pancreas, in which 30µl of 10^6 Panc02 cells suspension was injected using a 30 gauge insulin needle. All the organs were then returned to their original position and peritoneum and skin sutured. Animals were randomized after surgery into two treatment groups, the first receiving 250µg of α–CD20 antibody (Genentech, clone 5D2), the second receiving 250µg of the isotype-matched (IgG2a) irrelevant immunoglobulin (BioXCell C1.18.4), both with i.p. injection 3 days after surgery. After 3 weeks from surgery, mice were sacrificed and tumor masses collected. Single cell suspensions were obtained by incubating fragmented tumors with 0.5 mg/ml of clostridium histolyticum derived collagenase (Sigma Aldrich) for 30 minutes at 37°C. Cells were then washed and tumor infiltrating leukocytes purified by a 44%/66% Percoll (GE Healthcare life sciences)

gradient centrifugation. The purified leukocytes were washed and aliquoted for multicolor FACS analysis or RNA extraction. Alternatively, tissues were fixed for immunohistochemical analysis.
Pancreatic cancer–prone Pdx-Cre- $Kras^{G12D}$ mice (KC mice) were bred, maintained and treated at the saprophytic and pathogen-free animal facility of the Center for Experimental Research and Medical Studies (Torino, Italy), as previously described (39). Briefly KC mice were vaccinated at 36 weeks of age and every 3 weeks for a total of 3 rounds of vaccination. Vaccination was achieved by electroporation with 50 μg of plasmid (either mock vector or the human Enolase (ENO-1) encoding vector), as previously described (39). Mice of the same age were randomly assigned to control and treatment groups, and all groups were specifically treated concurrently. Mice were sacrificed 8 weeks after the last vaccination to perform histologic or immunohistochemical analyses.

Flow-cytometry
Absolute numbers of $CD19^+$, $CD3^+$, $CD11b^+$ cells were assessed by flow cytometry on peripheral blood leukocytes at day 0, 3, 7, 14 and 21 days from antibody injection. Trucount kit (BD Biosciences) was used to obtain absolute numbers. The following fluorophore-conjugated primary antibodies were used: anti-CD45 (BD Pharmingen 30-F11), anti-CD19 (eBiosciences eBio1D3), anti-CD3(eBiosciences 145-2C11), anti-CD11b (BioLegend M1/70). Sample acquisition was performed on a BD LSRFORTESSA (BD Biosciences) and data analyzed with FlowJo software.
FACS staining was performed as previously described for blood samples, with the following antibodies: CD8 (BioLegend 53-6.7), CD4 (BioLegend RM4-5), NK1.1 (eBiosciences PK136), CD44 (eBiosciences IM7), CD62L (eBiosciences MEL-14); and CD45, CD11b, Ly6G (BD Pharmingen 1A8), F4/80 (Serotech Cl: A3-1), B220 (BD Pharmingen RA3-6B2).

ACKNOWLEDGMENTS

This work was supported by the Humanitas Clinical and Research Center (grant Translation in Medical Oncology 2013 to FM and AZ), the Italian Ministry of University and Research, (FIRB grant RBAP11H2R9 to AM), Associazione Italiana Ricerca sul Cancro (AIRC 5x1000 IG-12182 to PA and FN; IG 15257 to FN); Fondazione Italiana Ricerca sul Cancro (FIRC fellowship 15041 to GDC). The funders had no role in study design, data collection and analysis, decision to publish, or preparation of the manuscript. Authors declare no conflict of interest.

AUTHOR CONTRIBUTIONS

G.F.C.; N.C.; S.S.; G.D.C.; P.C.; F.M: acquisition and interpretation of data. N.C.;G.C.; G.D.C.: statistical analysis. F.G.; R.M.; E.M.: development of methodology. G.C.; F.G.; C.R; A.Z.: surgical specimen collection and clinical database handling. N.C.; F.M.: writing of the manuscript. F.N; P.C.; G.C.; G.D.C.; A.Z.; P.A.; A.Man.: critical review of the manuscript. F.M.: study concept and design. All the Authors read and approved the final version of the manuscript.

REFERENCES

1. Siegel, R., J. Ma, Z. Zou, and A. Jemal. 2014. Cancer statistics, 2014. *CA Cancer J Clin* 64: 9-29.
2. Conroy, T., F. Desseigne, M. Ychou, O. Bouche, R. Guimbaud, Y. Becouarn, A. Adenis, J. L. Raoul, S. Gourgou-Bourgade, C. de la Fouchardiere, J. Bennouna, J. B. Bachet, F. Khemissa-Akouz, D. Pere-Verge, C. Delbaldo, E. Assenat, B. Chauffert, P. Michel, C. Montoto-Grillot, and M. Ducreux. 2011. FOLFIRINOX versus gemcitabine for metastatic pancreatic cancer. *N Engl J Med* 364: 1817-1825.
3. Clark, C. E., S. R. Hingorani, R. Mick, C. Combs, D. A. Tuveson, and R. H. Vonderheide. 2007. Dynamics of the immune reaction to pancreatic cancer from inception to invasion. *Cancer Res* 67: 9518-9527.
4. Vonderheide, R. H., and L. J. Bayne. 2013. Inflammatory networks and immune surveillance of pancreatic carcinoma. *Curr Opin Immunol* 25: 200-205.
5. Olive, K. P., M. A. Jacobetz, C. J. Davidson, A. Gopinathan, D. McIntyre, D. Honess, B. Madhu, M. A. Goldgraben, M. E. Caldwell, D. Allard, K. K. Frese, G. Denicola, C. Feig, C. Combs, S. P. Winter, H. Ireland-Zecchini, S. Reichelt, W. J. Howat, A. Chang, M. Dhara, L. Wang, F. Ruckert, R. Grutzmann, C. Pilarsky, K. Izeradjene, S. R. Hingorani, P. Huang, S. E. Davies, W. Plunkett, M. Egorin, R. H. Hruban, N. Whitebread, K. McGovern, J. Adams, C. Iacobuzio-Donahue, J. Griffiths, and D. A. Tuveson. 2009. Inhibition of Hedgehog signaling enhances delivery of chemotherapy in a mouse model of pancreatic cancer. *Science* 324: 1457-1461.
6. Ene-Obong, A., A. J. Clear, J. Watt, J. Wang, R. Fatah, J. C. Riches, J. F. Marshall, J. Chin-Aleong, C. Chelala, J. G. Gribben, A. G. Ramsay, and H. M. Kocher. 2013. Activated pancreatic stellate cells sequester CD8+ T cells to reduce their infiltration of the juxtatumoral compartment of pancreatic ductal adenocarcinoma. *Gastroenterology* 145: 1121-1132.
7. Beatty, G. L., E. G. Chiorean, M. P. Fishman, B. Saboury, U. R. Teitelbaum, W. Sun, R. D. Huhn, W. Song, D. Li, L. L. Sharp, D. A. Torigian, P. J. O'Dwyer, and R. H. Vonderheide. 2011. CD40 agonists alter tumor stroma and show efficacy against pancreatic carcinoma in mice and humans. *Science* 331: 1612-1616.
8. Ozdemir, B. C., T. Pentcheva-Hoang, J. L. Carstens, X. Zheng, C. C. Wu, T. R. Simpson, H. Laklai, H. Sugimoto, C. Kahlert, S. V. Novitskiy, A. De Jesus-Acosta, P. Sharma, P. Heidari, U. Mahmood, L. Chin, H. L. Moses, V. M. Weaver, A. Maitra, J. P. Allison, V. S. LeBleu, and R. Kalluri. 2014. Depletion of carcinoma-associated fibroblasts and fibrosis induces immunosuppression and accelerates pancreas cancer with reduced survival. *Cancer Cell* 25: 719-734.
9. Rhim, A. D., P. E. Oberstein, D. H. Thomas, E. T. Mirek, C. F. Palermo, S. A. Sastra, E. N. Dekleva, T. Saunders, C. P. Becerra, I. W. Tattersall, C. B. Westphalen, J. Kitajewski, M. G. Fernandez-Barrena, M. E. Fernandez-Zapico, C. Iacobuzio-Donahue, K. P. Olive, and B. Z. Stanger. 2014. Stromal elements act to restrain, rather than support, pancreatic ductal adenocarcinoma. *Cancer Cell* 25: 735-747.
10. Laheru, D., and E. M. Jaffee. 2005. Immunotherapy for pancreatic cancer - science driving clinical progress. *Nat Rev Cancer* 5: 459-467.
11. Erkan, M., S. Hausmann, C. W. Michalski, A. A. Fingerle, M. Dobritz, J. Kleeff, and H. Friess. 2012. The role of stroma in pancreatic cancer: diagnostic and therapeutic implications. *Nat Rev Gastroenterol Hepatol* 9: 454-467.
12. Ogino, S., J. Galon, C. S. Fuchs, and G. Dranoff. 2011. Cancer immunology--analysis of host and tumor factors for personalized medicine. *Nat Rev Clin Oncol* 8: 711-719.
13. Whiteside, T. L. 2013. Immune responses to cancer: are they potential biomarkers of prognosis? *Front Oncol* 3: 107.
14. Galon, J., H. K. Angell, D. Bedognetti, and F. M. Marincola. 2013. The continuum of cancer immunosurveillance: prognostic, predictive, and mechanistic signatures. *Immunity* 39: 11-26.
15. Galon, J., A. Costes, F. Sanchez-Cabo, A. Kirilovsky, B. Mlecnik, C. Lagorce-Pages, M. Tosolini, M. Camus, A. Berger, P. Wind, F. Zinzindohoue, P. Bruneval, P. H. Cugnenc, Z.

Trajanoski, W. H. Fridman, and F. Pages. 2006. Type, density, and location of immune cells within human colorectal tumors predict clinical outcome. *Science* 313: 1960-1964.
16. Di Caro, G., F. Bergomas, F. Grizzi, A. Doni, P. Bianchi, A. Malesci, L. Laghi, P. Allavena, A. Mantovani, and F. Marchesi. 2014. Occurrence of tertiary lymphoid tissue is associated with T-cell infiltration and predicts better prognosis in early-stage colorectal cancers. *Clin Cancer Res* 20: 2147-2158.
17. Fridman, W. H., F. Pages, C. Sautes-Fridman, and J. Galon. 2012. The immune contexture in human tumours: impact on clinical outcome. *Nat Rev Cancer* 12: 298-306.
18. Ogino, S., K. Nosho, N. Irahara, J. A. Meyerhardt, Y. Baba, K. Shima, J. N. Glickman, C. R. Ferrone, M. Mino-Kenudson, N. Tanaka, G. Dranoff, E. L. Giovannucci, and C. S. Fuchs. 2009. Lymphocytic reaction to colorectal cancer is associated with longer survival, independent of lymph node count, microsatellite instability, and CpG island methylator phenotype. *Clin Cancer Res* 15: 6412-6420.
19. Dieu-Nosjean, M. C., M. Antoine, C. Danel, D. Heudes, M. Wislez, V. Poulot, N. Rabbe, L. Laurans, E. Tartour, L. de Chaisemartin, S. Lebecque, W. H. Fridman, and J. Cadranel. 2008. Long-term survival for patients with non-small-cell lung cancer with intratumoral lymphoid structures. *J Clin Oncol* 26: 4410-4417.
20. Coppola, D., M. Nebozhyn, F. Khalil, H. Dai, T. Yeatman, A. Loboda, and J. J. Mule. 2011. Unique ectopic lymph node-like structures present in human primary colorectal carcinoma are identified by immune gene array profiling. *Am J Pathol* 179: 37-45.
21. Cipponi, A., M. Mercier, T. Seremet, J. F. Baurain, I. Theate, J. van den Oord, M. Stas, T. Boon, P. G. Coulie, and N. van Baren. 2012. Neogenesis of lymphoid structures and antibody responses occur in human melanoma metastases. *Cancer Res* 72: 3997-4007.
22. Di Caro, G., G. F. Castino, F. Bergomas, N. Cortese, M. Chiriva-Internati, F. Grizzi, A. Mantovani, and F. Marchesi. 2015. Tertiary lymphoid tissue in the tumor microenvironment: from its occurrence to immunotherapeutic implications. *Int Rev Immunol* 34: 123-133.
23. de Chaisemartin, L., J. Goc, D. Damotte, P. Validire, P. Magdeleinat, M. Alifano, I. Cremer, W. H. Fridman, C. Sautes-Fridman, and M. C. Dieu-Nosjean. 2011. Characterization of chemokines and adhesion molecules associated with T cell presence in tertiary lymphoid structures in human lung cancer. *Cancer Res* 71: 6391-6399.
24. Junt, T., E. Scandella, and B. Ludewig. 2008. Form follows function: lymphoid tissue microarchitecture in antimicrobial immune defence. *Nat Rev Immunol* 8: 764-775.
25. Neyt, K., F. Perros, C. H. GeurtsvanKessel, H. Hammad, and B. N. Lambrecht. 2012. Tertiary lymphoid organs in infection and autoimmunity. *Trends Immunol* 33: 297-305.
26. Goc, J., C. Germain, T. K. Vo-Bourgais, A. Lupo, C. Klein, S. Knockaert, L. de Chaisemartin, H. Ouakrim, E. Becht, M. Alifano, P. Validire, R. Remark, S. A. Hammond, I. Cremer, D. Damotte, W. H. Fridman, C. Sautes-Fridman, and M. C. Dieu-Nosjean. 2014. Dendritic Cells in Tumor-Associated Tertiary Lymphoid Structures Signal a Th1 Cytotoxic Immune Contexture and License the Good Positive Prognostic Value of Infiltrating CD8+ T Cells. *Cancer Res*
27. de Visser, K. E., L. V. Korets, and L. M. Coussens. 2005. De novo carcinogenesis promoted by chronic inflammation is B lymphocyte dependent. *Cancer Cell* 7: 411-423.
28. Ammirante, M., J. L. Luo, S. Grivennikov, S. Nedospasov, and M. Karin. 2010. B-cell-derived lymphotoxin promotes castration-resistant prostate cancer. *Nature* 464: 302-305.
29. Schioppa, T., R. Moore, R. G. Thompson, E. C. Rosser, H. Kulbe, S. Nedospasov, C. Mauri, L. M. Coussens, and F. R. Balkwill. 2011. B regulatory cells and the tumor-promoting actions of TNF-alpha during squamous carcinogenesis. *Proc Natl Acad Sci U S A* 108: 10662-10667.
30. Coussens, L. M., L. Zitvogel, and A. K. Palucka. 2013. Neutralizing tumor-promoting chronic inflammation: a magic bullet? *Science* 339: 286-291.
31. Affara, N. I., B. Ruffell, T. R. Medler, A. J. Gunderson, M. Johansson, S. Bornstein, E. Bergsland, M. Steinhoff, Y. Li, Q. Gong, Y. Ma, J. F. Wiesen, M. H. Wong, M. Kulesz-Martin, B. Irving, and L. M. Coussens. 2014. B cells regulate macrophage phenotype and response to chemotherapy in squamous carcinomas. *Cancer Cell* 25: 809-821.
32. Shalapour, S., J. Font-Burgada, G. Di Caro, Z. Zhong, E. Sanchez-Lopez, D. Dhar, G. Willimsky, M. Ammirante, A. Strasner, D. E. Hansel, C. Jamieson, C. J. Kane, T. Klatte, P. Birner, L. Kenner, and M. Karin. 2015. Immunosuppressive plasma cells impede T-cell-

dependent immunogenic chemotherapy. *Nature*
33. Schaerli, P., K. Willimann, A. B. Lang, M. Lipp, P. Loetscher, and B. Moser. 2000. CXC chemokine receptor 5 expression defines follicular homing T cells with B cell helper function. *J Exp Med* 192: 1553-1562.
34. Breitfeld, D., L. Ohl, E. Kremmer, J. Ellwart, F. Sallusto, M. Lipp, and R. Forster. 2000. Follicular B helper T cells express CXC chemokine receptor 5, localize to B cell follicles, and support immunoglobulin production. *J Exp Med* 192: 1545-1552.
35. Vinuesa, C. G., S. G. Tangye, B. Moser, and C. R. Mackay. 2005. Follicular B helper T cells in antibody responses and autoimmunity. *Nat Rev Immunol* 5: 853-865.
36. Good-Jacobson, K. L., C. G. Szumilas, L. Chen, A. H. Sharpe, M. M. Tomayko, and M. J. Shlomchik. 2010. PD-1 regulates germinal center B cell survival and the formation and affinity of long-lived plasma cells. *Nat Immunol* 11: 535-542.
37. Chevalier, N., D. Jarrossay, E. Ho, D. T. Avery, C. S. Ma, D. Yu, F. Sallusto, S. G. Tangye, and C. R. Mackay. 2011. CXCR5 expressing human central memory CD4 T cells and their relevance for humoral immune responses. *J Immunol* 186: 5556-5568.
38. Gu-Trantien, C., S. Loi, S. Garaud, C. Equeter, M. Libin, A. de Wind, M. Ravoet, H. Le Buanec, C. Sibille, G. Manfouo-Foutsop, I. Veys, B. Haibe-Kains, S. K. Singhal, S. Michiels, F. Rothe, R. Salgado, H. Duvillier, M. Ignatiadis, C. Desmedt, D. Bron, D. Larsimont, M. Piccart, C. Sotiriou, and K. Willard-Gallo. 2013. CD4(+) follicular helper T cell infiltration predicts breast cancer survival. *J Clin Invest* 123: 2873-2892.
39. Cappello, P., S. Rolla, R. Chiarle, M. Principe, F. Cavallo, G. Perconti, S. Feo, M. Giovarelli, and F. Novelli. 2013. Vaccination with ENO1 DNA prolongs survival of genetically engineered mice with pancreatic cancer. *Gastroenterology* 144: 1098-1106.
40. Gajewski, T. F., H. Schreiber, and Y. X. Fu. 2013. Innate and adaptive immune cells in the tumor microenvironment. *Nat Immunol* 14: 1014-1022.
41. Dieu-Nosjean, M. C., J. Goc, N. A. Giraldo, C. Sautes-Fridman, and W. H. Fridman. 2014. Tertiary lymphoid structures in cancer and beyond. *Trends Immunol* 35(11): 571-580.
42. Germain, C., S. Gnjatic, F. Tamzalit, S. Knockaert, R. Remark, J. Goc, A. Lepelley, E. Becht, S. Katsahian, G. Bizouard, P. Validire, D. Damotte, M. Alifano, P. Magdeleinat, I. Cremer, J. L. Teillaud, W. H. Fridman, C. Sautes-Fridman, and M. C. Dieu-Nosjean. 2014. Presence of B Cells in Tertiary Lymphoid Structures is Associated with a Protective Immunity in Lung Cancer Patients. *Am J Respir Crit Care Med*
43. Thaunat, O., N. Patey, C. Gautreau, S. Lechaton, V. Fremeaux-Bacchi, M. C. Dieu-Nosjean, E. Cassuto-Viguier, C. Legendre, M. Delahousse, P. Lang, J. B. Michel, and A. Nicoletti. 2008. B cell survival in intragraft tertiary lymphoid organs after rituximab therapy. *Transplantation* 85: 1648-1653.
44. Vinuesa, C. G., and J. G. Cyster. 2011. How T cells earn the follicular rite of passage. *Immunity* 35: 671-680.
45. Schietinger, A., and P. D. Greenberg. 2013. Tolerance and exhaustion: defining mechanisms of T cell dysfunction. *Trends Immunol*
46. Topalian, S. L., C. G. Drake, and D. M. Pardoll. 2012. Targeting the PD-1/B7-H1(PD-L1) pathway to activate anti-tumor immunity. *Curr Opin Immunol* 24: 207-212.
47. Gros, A., P. F. Robbins, X. Yao, Y. F. Li, S. Turcotte, E. Tran, J. R. Wunderlich, A. Mixon, S. Farid, M. E. Dudley, K. Hanada, J. R. Almeida, S. Darko, D. C. Douek, J. C. Yang, and S. A. Rosenberg. 2014. PD-1 identifies the patient-specific CD8(+) tumor-reactive repertoire infiltrating human tumors. *J Clin Invest* 124: 2246-2259.
48. Zheng, L., J. Xue, E. M. Jaffee, and A. Habtezion. 2013. Role of immune cells and immune-based therapies in pancreatitis and pancreatic ductal adenocarcinoma. *Gastroenterology* 144: 1230-1240.
49. Bazhin, A. V., I. Shevchenko, V. Umansky, J. Werner, and S. Karakhanova. 2014. Two immune faces of pancreatic adenocarcinoma: possible implication for immunotherapy. *Cancer Immunol Immunother* 63: 59-65.
50. Messina, J. L., D. A. Fenstermacher, S. Eschrich, X. Qu, A. E. Berglund, M. C. Lloyd, M. J. Schell, V. K. Sondak, J. S. Weber, and J. J. Mule. 2012. 12-Chemokine gene signature identifies lymph node-like structures in melanoma: potential for patient selection for immunotherapy? *Sci Rep* 2: 765.

51. Lutz, E. R., A. A. Wu, E. Bigelow, R. Sharma, G. Mo, K. Soares, S. Solt, A. Dorman, A. Wamwea, A. Yager, D. Laheru, C. L. Wolfgang, J. Wang, R. H. Hruban, R. A. Anders, E. M. Jaffee, and L. Zheng. 2014. Immunotherapy converts nonimmunogenic pancreatic tumors into immunogenic foci of immune regulation. *Cancer Immunol Res* 2: 616-631.
52. Altman, D. G., L. M. McShane, W. Sauerbrei, and S. E. Taube. 2012. Reporting Recommendations for Tumor Marker Prognostic Studies (REMARK): explanation and elaboration. *PLoS Med* 9: e1001216.

Table 1. Predictors of post-surgical disease specific survival in 104 patients with pancreatic ductal adenocarcinoma

		Univariate Analysis [a]		Multivariate Analysis [a]	
		H.R. (95%C.I.)	P	H.R. (95%C.I.)	P
Patient Demographics					
Age	< 50 yrs	1.00 ref.			
	50-70 yrs	2.13 (0.49-9.29)	0.312		
	≥ 70 yrs	4.22 (0.98-18.13)	0.053		
Gender	Female	1.00 ref.			
	Male	1.09 (0.58-2.07)	0.782		
Tumor Features					
Nodal involvement	No	1.00 ref.		1.00 ref.	
	Yes	2.13(1.03-4.41)	**0.020**	2.63 (1.17-5.90)	**0.019**
	na				
Grade [c]	G1/G2	1.00 ref.		1.00 ref.	
	G3/G4	2.74 (1.37-5.49)	**0.004**	2.50 (1.20-5.24)	**0.015**
	na				
Radical surgery	No	1.96 (0.93-4.14)	0.078		
	Yes	1.00 ref			
	na				
Chemotherapy (CTX)					
Adjuvant treatment	No	1.00 ref			
	Yes	1.03 (0.52-2.04)	0.942		
Tumor Immune features					
CD20-TLT (quartiles)[b]	1st (0-1.71)	1.00 ref.		1.00 ref.	
	2nd (1.71-3.72)	0.40 (0.16-0.98)	**0.045**	0.41 (0.15-1.09)	0.075
	3rd (3.72-5.71)	0.38 (0.16-0.94)	**0.035**	0.25 (0.09-0.72)	**0.011**
	4th (5.71-23.49)	0.40 (0.16-0.98)	**0.044**	0.26 (0.09-0.72)	**0.010**
CD20-TILs (quartiles)[b]	1st (0-0.26)	1.00 ref.		1.00 ref.	
	2nd (0.26-0.41)	1.30 (0.50-3.36)	0.594	1.49 (0.53-4.19)	0.449
	3rd (0.41-0.69)	2.88 (1.18-7.03)	**0.020**	2.85 (1.05-7.78)	**0.040**
	4th (0.69-1.89)	1.23 (0.46-3.30)	0.674	1.88 (0.58-6.03)	0.289
CD8-TILs (quartiles) [b]	1st (0.0-0.34)	1.00 ref.			
	2nd (0.34-0.61)	0.51 (0.22-1.23)	0.135		
	3rd (0.61-1.15)	0.89 (0.39-2.07)	0.797		
	4th (1.15-3.42)	0.69 (0.27-1.77)	0.445		
PD-1 GC	Yes	1.00 ref.			
	No	1.47 (0.72-2.99)	0.285		

[a] COX regression analysis
[b] Densities as percent immunoreactive area at the tumor-stroma interface
[c] G1/G2, well-to moderately differentiated; G3, G4 poorly differentiated

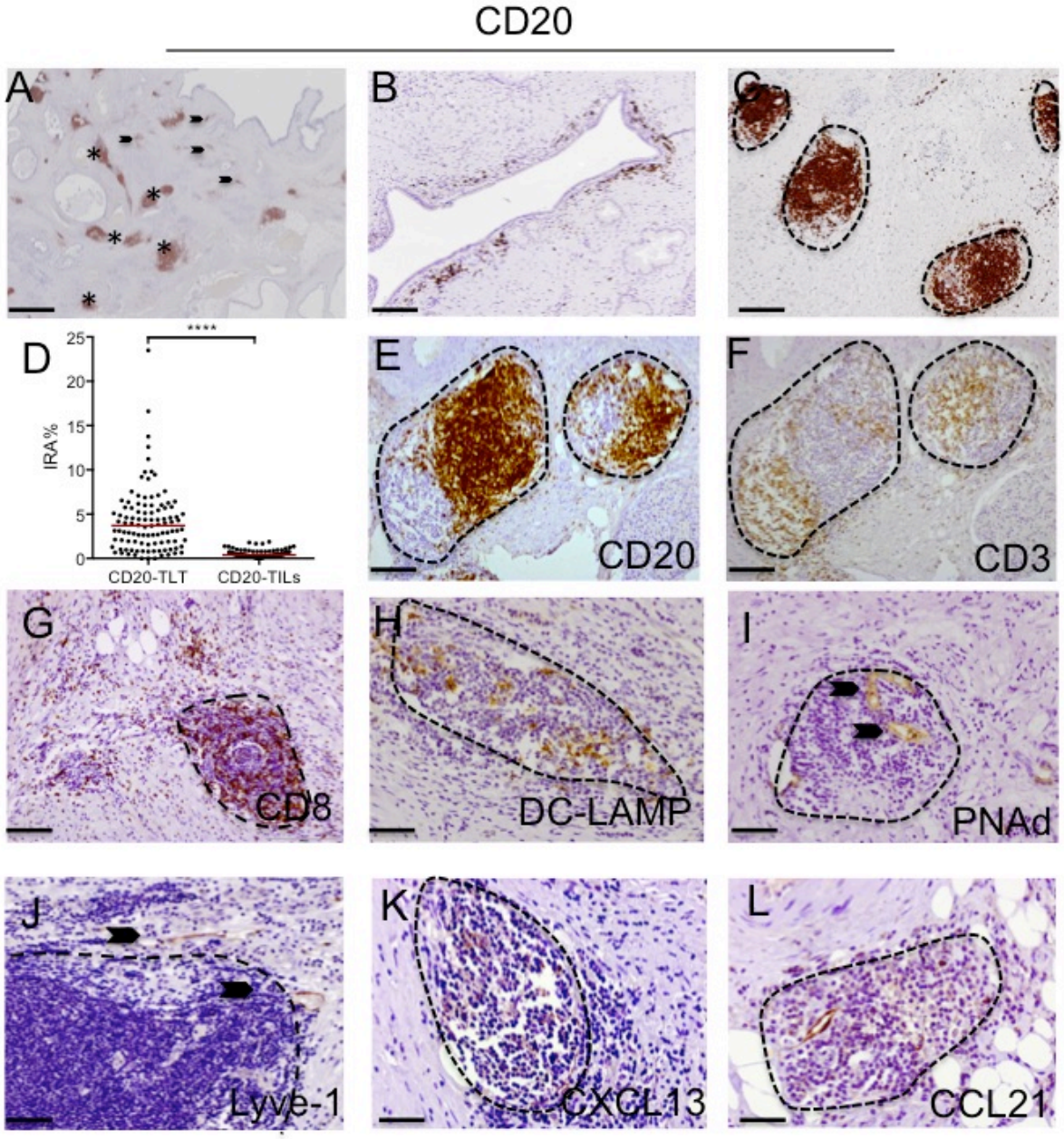

Figure 1. B cells strategically localize in tertiary lymphoid tissue in human pancreatic adenocarcinoma. (A-C) Histological sections of human PDAC, stained for $CD20^+$ B cells. A representative image obtained from a virtual digital slide of a human PDAC specimen; staining with an anti-CD20 antibody shows few B cells distributed at the tumor margin (arrowheads in **A** and **B**) and the majority of B cells located within dense aggregates (asterisks in **A** and **C**). **(D)** Quantitative evaluation of the density of B cells according to their localization within CD20-TLT or as CD20-TILs in tissue specimens from 104 PDAC patients. Density of B cells in TLT (CD20-TLT IRA%) was significantly higher compared to density of scattered CD20-TILs (CD20-TILs IRA%) (****: P<0.0001 by Student's t test). (**E-L**) Lymph-node like aggregates (dotted lines) in human PDAC specimens are composed of $CD20^+$ B cells (**E**), $CD3^+$ T cells (**F**) and mature dendritic cells expressing DC-LAMP (**G**). Sections in **E** and **F** panels are consecutive and show the topological compartmentalization of B and T cells. An organized network of specialized $PNAd^+$ high endothelial venules (HEV) (**H**) and Lyve-1^+ lymphatics (**J**) confirms that the aggregates have features of tertiary lymphoid tissue (TLT). The lymphoid chemokines CXCL13 (**K**) and CCL21 (**L**) are present

inside lymphoid aggregates. Dotted lines indicate follicle contour. Bars: (A) 500 μm, (B-G) 200 μm, (H-L) 100 μm.

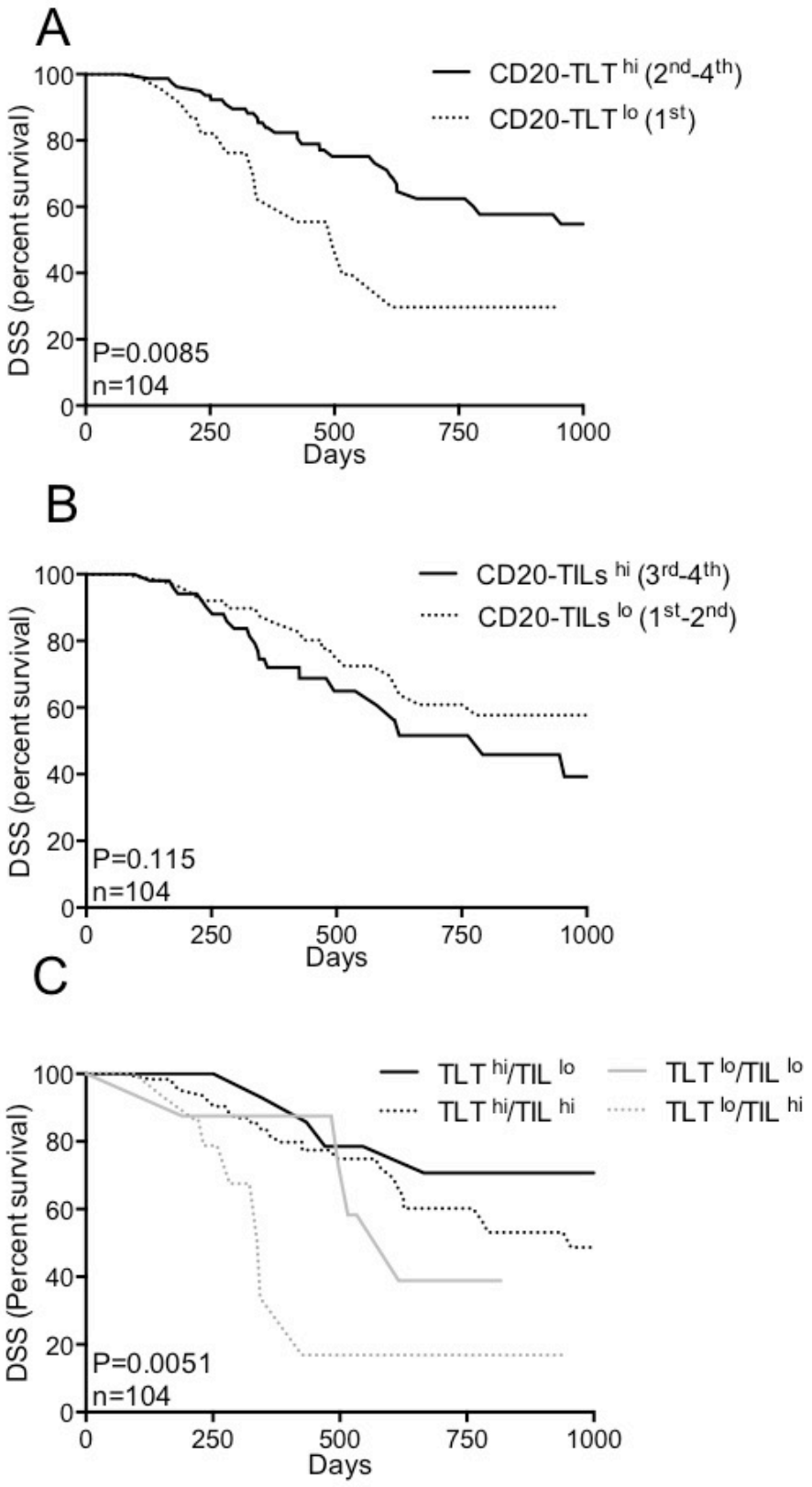

Figure 2. Clinical relevance of B cells according to their distribution in human PDAC. (**A-C**) Distinct spatial localization of B cells in the tumor microenvironment dictates their prognostic behavior. Kaplan-Meier survival analyses shows correlation of high density of CD20-TLT (2^{nd}-4^{th} quartiles) with longer disease specific survival (P=0.0085; n=104) (**A**), while high density of CD20-TILs (3^{rd}-4^{th} quartiles) shows a tendency to associate to worse prognosis (P=0.115; n=104) (**B**). The immune signature comprising CD20- TLT^{hi} /CD20- TIL^{lo} robustly predicts longer survival (P=0.0051; n=104) (**C**). P value by Wilcoxon-Mantle Cox test.

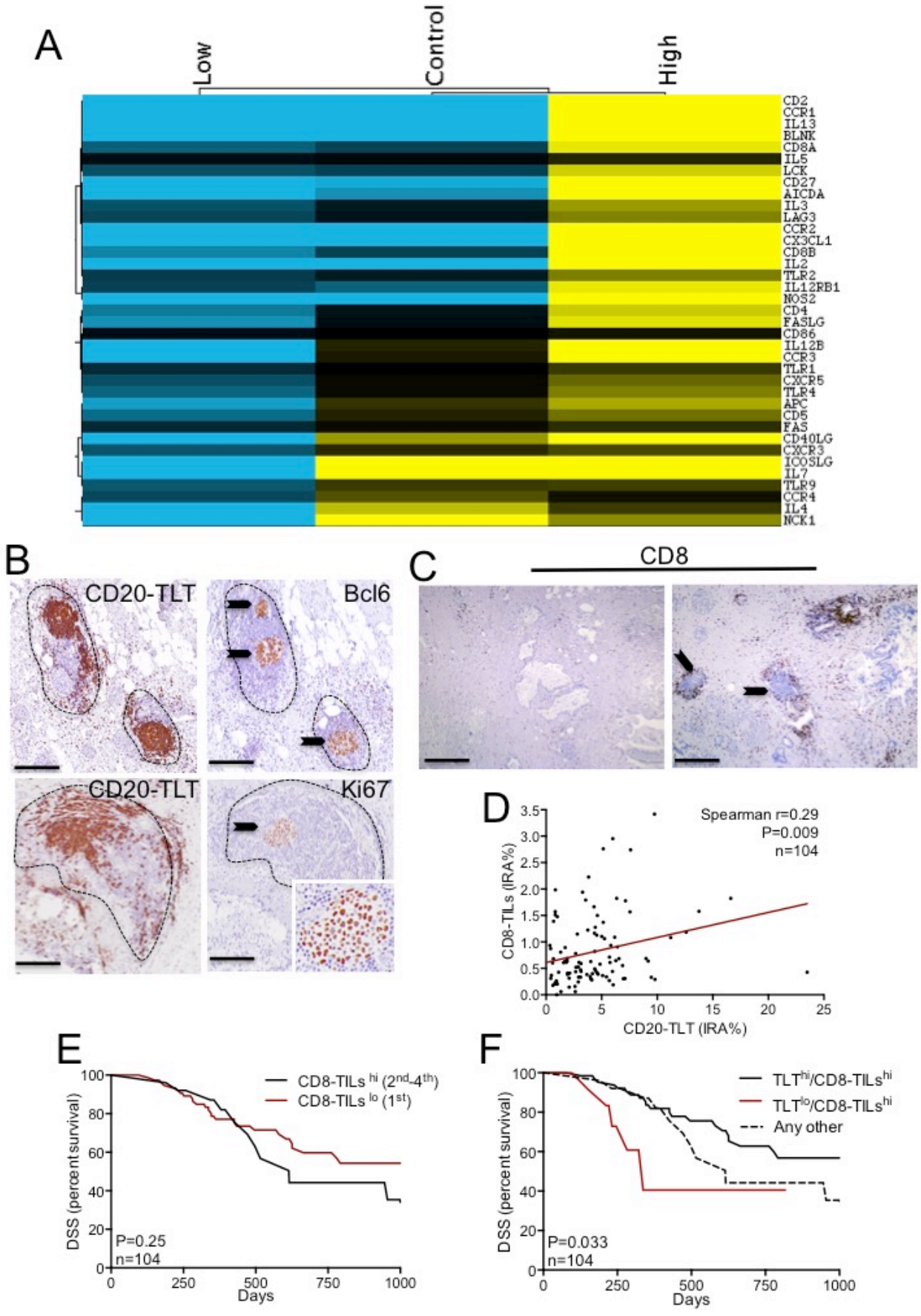

Figure 3. Confinement of B cells within TLT associates to a specific immune signature, correlates with CD8-TIL infiltration, and empowers the favourable prognostic value of CD8-TILs. (**A**) Heatmap analysis showing the immune signature of human PDAC specimens with

different CD20-TLT density. RNA was extracted from paraffin embedded tissue specimens of human PDAC, categorized as TLT^{hi} (n=3) or TLT^{lo}(n=3) after immunohistochemical evaluation with an anti CD20 antibody. RNA from normal pancreata (n=3) was obtained as a control. Stable grouping followed the pattern of B cell distribution (i.e. TLT^{hi} versus TLT^{lo} samples segregating together), suggesting that B cell infiltration identifies specific gene expression programs. (**B**) Presence of germinal center in CD20-TLT. B cells within TLT are engaged in a germinal center reaction, as evidenced by Bcl-6 (arrowheads in upper right panel) and Ki-67 (arrowhead in lower right panel) staining within CD20-TLT (left panel). Left and right sections are consecutive sections. (**C-F**) CD20-TLT correlates with density of $CD8^+$ T cells in human PDAC and empowers their prognostic function. Representative images obtained from virtual digital slides of human PDAC specimens stained with an anti-CD8 antibody show a high density of CD8+ cells (**C**). Density of CD20-TLT (IRA%) linearly correlates with density of CD8-TILs (IRA%) (r=0.29, p=0.009, n=104) (**D**). (**E**) Kaplan-Meier curve showing that while high density of CD8-TILs (2^{nd}-4^{th} quartiles) is not significantly associated to prognosis (P=0.254, n=104), concomitant high density of CD8-TILs (2^{nd}-4^{th} quartiles) and high density of CD20-TLT (2^{nd}-4^{th} quartiles) identifies a subgroup of patients with longer disease-specific survival (P=0.031; n=104) (**F**). P value by Pearson's simple linear regression analysis in (**D**) and by Wilcoxon-Mantle Cox test in (**E-F**). Bars: 200 μm (**B**); 500 μm (**C**).

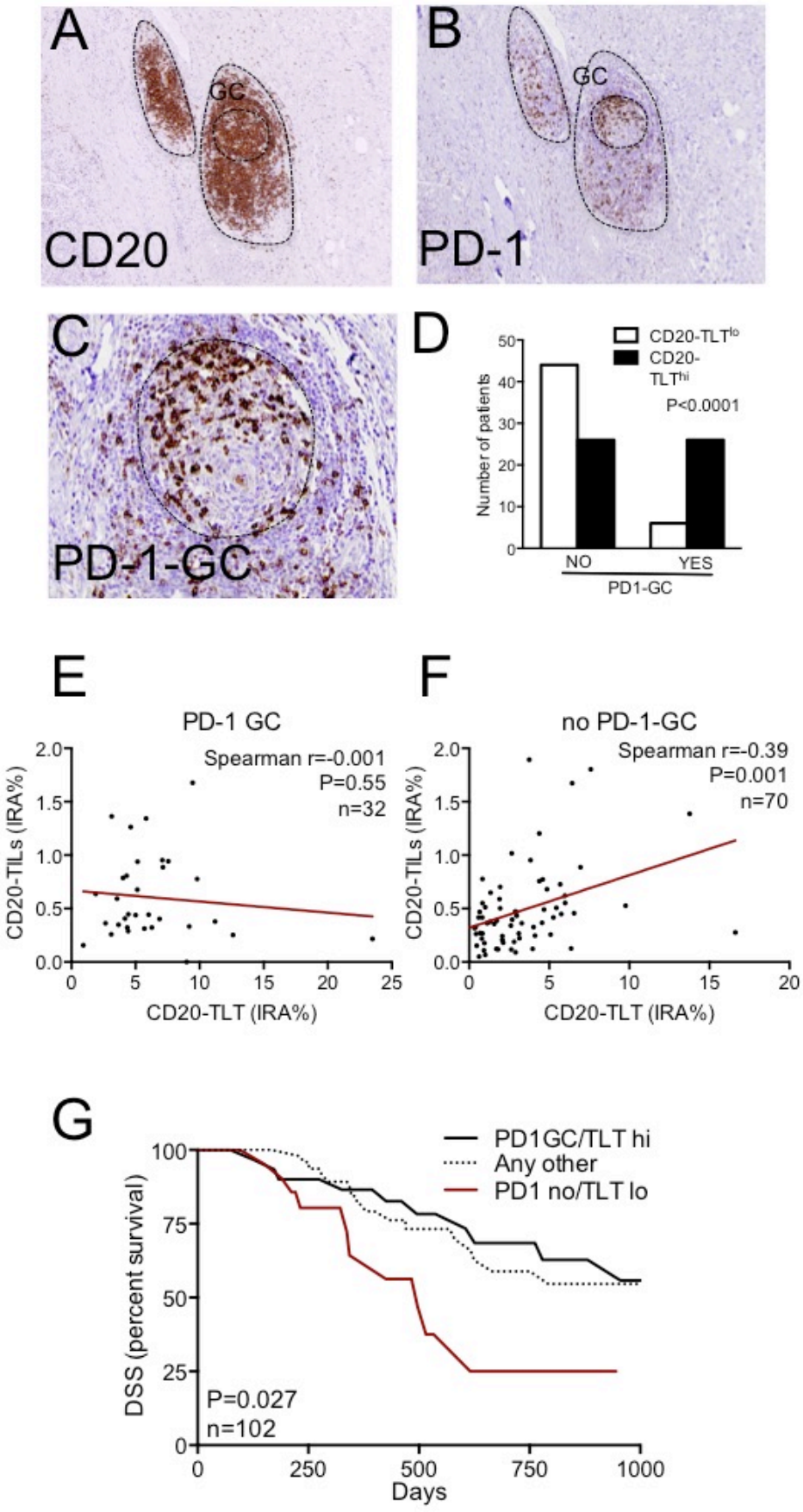

Figure 4. PD-1$^+$ follicular helper T cells within TLT germinal centers regulate the balance between B-cell protumor and antitumor prognostic value. (A-C) Presence of PD-1$^+$ cells within germinal centers of CD20-TLT in human PDAC. Within the B-cell zone of TLT (**A**), there are PD-1$^+$

cells (**B**), some of which distributed in the germinal center, suggesting they could be T-helper follicular cells (**C**). (**D**) The number of patients with high density of TLT is significantly higher in the PD1-GC group compared to specimens with low density of TLT ($p<0.0001$). (**E-F**) Lack of correlation of CD20-TLT and CD20-TILs in patients with PD-1-GC ($r=-0.001$, $P=0.559$, $n=32$) (**E**), while the two B cell components correlate in specimens without PD1-GC ($r=0.39$, $P=0.001$, $n=70$) (**F**), suggesting that the presence of PD1-GC cells could be an important factor favoring B cell aggregation in TLT and preventing B cell scattering within the tissue. (**G**) A concomitant presence of PD1-GC cells and high TLT (2^{nd}-4^{th} quartiles) identified a subgroup of patients with a significantly better prognosis ($p=0.027$, $n=102$). P value by Chi-square in (**D**), Pearson's simple linear regression analysis in (**E-F**) and by Wilcoxon-Mantle Cox test in (**G**). Bars: 200 μm (**A-B**); 50 μm (**C**).

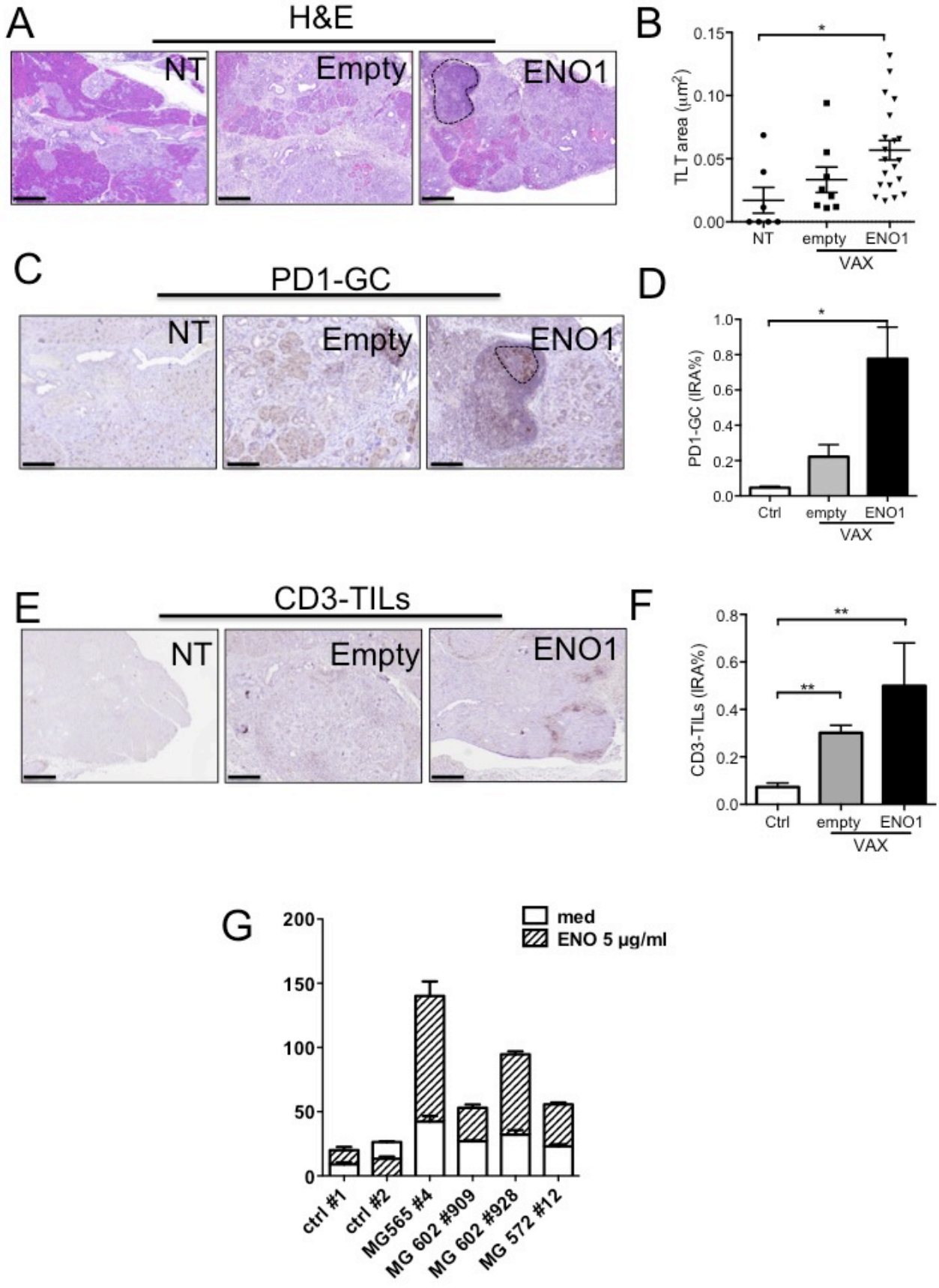

Figure 5. An immunotherapeutic DNA-vaccine induces neogenesis of intratumor TLT with active germinal centers in a preclinical model of PDAC. (**A-F**) Induction of TLT by an antitumor

vaccination in Pdx-Cre- $Kras^{G12D}$ mice. Histological sections of murine PDAC from non treated mice (NT) or mice vaccinated with empty vector (empty) or a vector encoding ENO1 (ENO1) stained with hematoxylin-eosin (**A**), PD-1 (**C**), CD3 (**E**). Dotted line indicates an intratumor TLT (**A**) or PD1-GC (**C**). Number and area of TLT (**B**), IRA% of PD1-GC (**D**) and CD3-TILs (**F**) are significantly increased by vaccination compared to untreated mice. (**G**) ENO1 vaccination induces humoral response. Spleen cells from empty plasmid (white bars) or ENO1 plasmid-vaccinated (squared bars) mice were stimulated on an enzyme-linked immunosorbent spot plate with rENO1. Anti-ENO1 antibodies are significantly induced in ENO1-vaccinated KC mice, but not in mice vaccinated with the empty vector. Numbers in the graph represent the mean number of specific spots subtracted from that of background. All conditions were in quadruplicate. P value by Students' t test. *: $P<0.05$; **:$P<0.01$. Scale bar 500 μm.

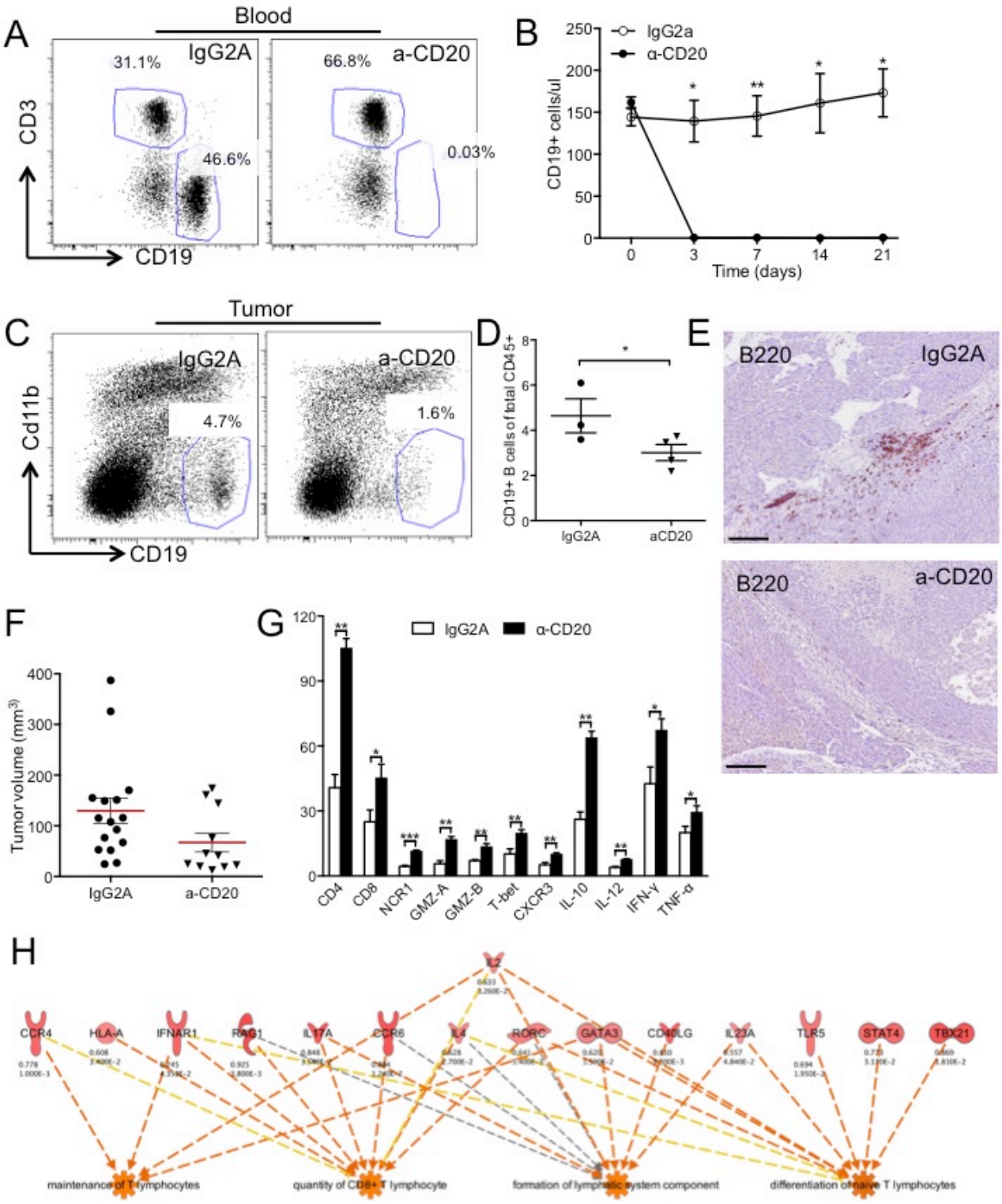

Figure 6. Targeting tumor infiltrating B cells unleashes immune response in murine PDAC. (A-F) Depletion of B cells by an anti-CD20 antibody in a murine implantable PDAC model. Mice were orthotopically injected with the PDAC cell line Panc02 and administered either irrelevant antibody (IgG2A) or a-CD20 on day 3 post injection. (**A**) Exemplificative facs plot showing depletion of circulating blood CD19+ B cells. (**B**) B cell depletion started at day 3 and lasted until

the end of the experiment. One independent experiment repeated 3 times is shown (n = 3 mice, IgG2A; n = 4 mice a-CD20; bars represent SEM; *:P<0.05; **:P<0.01). (**C**) Exemplificative facs plot showing depletion of tumor infiltrating CD19+ B cells. (**D**) Percentage of CD19+ B cells infiltrating PDAC tumors is reduced by a-CD20 treatment. One exemplificative of three experiments performed is shown (n = 3 mice, IgG2A; n = 4 mice a-CD20; bars represent SEM; P=0.084 by Students' t test. **(E)** Immunohistochemical evaluation of B cells in PDAC. Representative pictures showing reduction of B-TILs in the pancreas of a-CD20 treated mice. (**F**) Tumor growth was slightly but not significantly reduced by a-CD20 treatment. (**G-H**) Immune signature after a-CD20 treatment. RNA from leukocytes isolated from PDAC of mice treated with IgG2A or a-CD20 shows induction of genes related to T cell infiltration and activation (**G**). Systems biology analysis of the genes modulated after depletion of B cells highlights significant enrichment of biological functions related to lymphoid tissue structure and development, CD8+ T cell infiltration and maintenance and differentiation of T cells (**H**).